



**CHALMERS**  
UNIVERSITY OF TECHNOLOGY

## **First-Principles Estimation of Thermodynamic Properties and Phase Stability of $\text{CaMnO}_{3-\delta}$ for Chemical-Looping Combustion**

Downloaded from: <https://research.chalmers.se>, 2026-05-16 05:47 UTC

Citation for the original published paper (version of record):

Gastaldi, J., Brorsson, J., Stanicic, I. et al (2025). First-Principles Estimation of Thermodynamic Properties and Phase Stability of  $\text{CaMnO}_{3-\delta}$  for Chemical-Looping Combustion. *Energy & Fuels*, 39(19): 9113-9120. <http://dx.doi.org/10.1021/acs.energyfuels.5c00267>

N.B. When citing this work, cite the original published paper.

# First-Principles Estimation of Thermodynamic Properties and Phase Stability of $\text{CaMnO}_{3-\delta}$ for Chemical-Looping Combustion

Jonatan Gastaldi,\* Joakim Brorsson, Ivana Stanić, Anders Hellman, and Tobias Mattisson



Cite This: *Energy Fuels* 2025, 39, 9113–9120



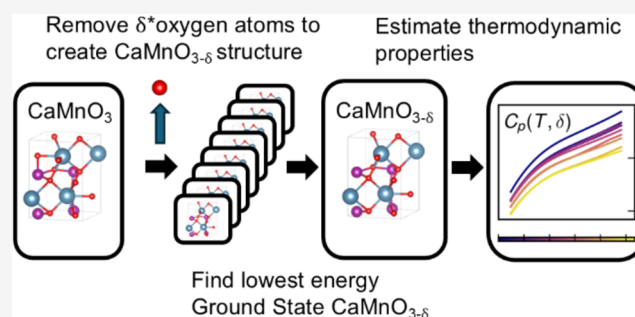
Read Online

ACCESS |

Metrics & More

Article Recommendations

**ABSTRACT:** Chemical-looping is a technology that increases combustion efficiency and enables carbon capture with a low energy penalty. A central component in chemical-looping is the oxygen carrier particles, which transfer oxygen from the air reactor to the fuel reactor. It is, therefore, important to look for new materials that might perform better than those used today. How suitable a material is as an oxygen carrier is largely determined by its thermodynamic properties, as this governs the maximum extent of fuel conversion in the fuel reactor. Gathering data to estimate thermodynamic properties is sometimes difficult or even impossible using experimental methods.  $\text{CaMnO}_{3-\delta}$  is an example of a complex material that has shown promise as an oxygen carrier for chemical-looping combustion and chemical-looping with oxygen uncoupling. Still, the fundamentals of this system are not fully understood, and available thermodynamic data show significant variations. Computational modeling is a method for generating thermodynamic data of equivalent accuracy to experimental investigations for complex systems. In this study, first-principles calculations by using density functional theory (DFT) and three different functionals (GGA + U, SCAN,  $r^2$ SCAN) have been used to investigate the perovskite  $\text{CaMnO}_{3-\delta}$ . Our unique approach allows for the detailed examination of individual oxygen vacancies and their impact on thermodynamic properties, which is critical for understanding oxygen transport in chemical-looping. This is important since vacancies largely govern the oxygen transport needed in chemical-looping. The generated data is used in multiphase thermodynamic calculations to achieve greater detail in the predicted Ca–Mn–O phase-diagrams. The calculated results using SCAN show good agreement with data found in commercial databases and experimental data when comparing heat capacity and entropy, with differences of  $-1.17$  and  $-11.17$  J/(molK), respectively, for  $\delta = 0$  and 298.15 K. However, a larger discrepancy is shown for the estimated formation enthalpy at the same conditions,  $+26$  kJ/mol compared to data from a commercial database. The results using  $r^2$ SCAN are within 0.5% of the results using SCAN. The functional GGA + U estimates larger differences than SCAN and  $r^2$ SCAN,  $+0.77$ ,  $-5.43$  J/(molK), and  $+48$  kJ/mol for heat capacity, entropy and formation enthalpy, respectively. This indicates that  $\text{CaMnO}_3$  is less stable than previously proposed in the literature.



## 1. INTRODUCTION

Climate change has been, and still is, one of the greatest challenges facing humanity. It has been proven to be driven primarily by human-made additions of greenhouse gases (GHG), including  $\text{CO}_2$  and  $\text{CH}_4$ . The most recent report from IPCC<sup>1</sup> shows that the amount of GHGs in the atmosphere is still increasing and that it will be difficult to keep the temperature rise to less than  $1.5$  °C, which was the goal set in the Paris Agreement.<sup>2</sup> Estimates show that in order to keep the increase below  $2$  °C, it will be necessary to achieve negative emissions by collecting  $\text{CO}_2$  from the atmosphere.<sup>3,4</sup> The increasing levels of GHGs indicate that it is difficult to completely phase out fuel combustion as an energy source. A solution to this problem is to develop technologies for cheap capture and sequestering of  $\text{CO}_2$  after combustion. A potential alternative for this type of technology is chemical-looping combustion (CLC), which makes it possible to perform the

combustion without any dilution with nitrogen from the air. This is achieved by using an oxygen carrier to transfer oxygen from the air reactor to the fuel reactor. As a result, only two components,  $\text{CO}_2$  and  $\text{H}_2\text{O}$ , need to be separated post-combustion by simple condensation, which reduces the cost of capturing the  $\text{CO}_2$ . If the fuel being used in this process is an environmentally sourced biomass, CLC can be used to realize the concept of bioenergy with carbon capture and storage (BECCS).<sup>5</sup> In particular, this allows heat and power to be

Received: January 14, 2025

Revised: April 17, 2025

Accepted: April 18, 2025

Published: April 30, 2025



efficiently generated while achieving negative emissions of CO<sub>2</sub>.

Oxygen is absorbed in the so-called air reactor and transported by oxygen carrier (OC) particles into the fuel reactor, where the combustion takes place. Critically, the particles are circulated back into the air reactor to be reoxidized after releasing oxygen inside the fuel reactor. This means that the OC must be able to transfer oxygen to the fuel in a way that suppresses the formation of unwanted byproducts. It should also be able to undergo multiple oxidation and reduction cycles without breaking apart. One of the most common OCs today is ilmenite, which can be seen as a benchmark oxygen carrier and used in most pilot operations.<sup>6,7</sup> While this material is both relatively potent and cost-effective, there are ongoing efforts to find even better alternatives, both among natural ores and synthetic metal oxides.

Theoretical models can be used to estimate the inherent properties of materials as well as their effect on macro-scale phenomena, for instance, the ability to function as an OC. Thermodynamic calculations are widely used to understand chemical processes such as CLC. Here it is important as thermodynamic equilibrium largely governs the extent to which a fuel can be converted to CO<sub>2</sub> and H<sub>2</sub>O.<sup>8</sup> This is given by the partial pressure of oxygen over the oxygen carrier material, and it can also be expected that the oxygen transport rate is governed by the difference in oxygen partial pressure on the particle surface and the bulk gas concentration. However, a profound limitation of most theoretical models is the need for experimental data. When data is missing or cannot be attained experimentally, a potential solution is to generate the required information using first-principles calculations. Such predictions can then be used together with the known data to explain experimental observations. For example, this is useful for chemical-looping since it enables a detailed analysis of the interactions between OCs and fuels at high temperatures.

OCs are typically oxides of transition metals such as Fe,<sup>7</sup> Mn,<sup>9–11</sup> and Cu<sup>12,13</sup> that have all been shown to work but also suffer from at least some drawbacks. Oxides containing Cu, for instance, are expensive and tend to agglomerate,<sup>12</sup> while those containing Mn<sup>12</sup> have shown problems during the reoxidation in the air reactor.

In recent years, perovskites have been found to be promising OCs in CLC.<sup>14–17</sup> These structures can be represented by the general formula ABO<sub>3-δ</sub>, where A is a larger alkali or rare earth cation, and B is a smaller transition metal cation. This type of materials transfer oxygen within the same phase, unlike common monometallic oxygen carriers, a phenomenon which manifests itself in a nonstoichiometric phase. Since multiple species can partially occupy both sites, the number of potential combinations is enormous. One such perovskite, which has been extensively investigated, is CaMnO<sub>3-δ</sub>.<sup>11,15,18</sup> Besides showing promising results in CLC processes, Ca- and Mn-oxides are cheap and abundant on the market making CaMnO<sub>3-δ</sub> cheaper to synthesize than other synthesizable OCs.<sup>11</sup> One major problem, however, is the long-term stability since it tends to undergo an irreversible phase change to CaMn<sub>2</sub>O<sub>4</sub> and Ca<sub>2</sub>MnO<sub>4</sub>.<sup>12</sup> These phases are not beneficial to CLC since they do not possess the same redox properties as CaMnO<sub>3-δ</sub>.<sup>14</sup> It has been found that replacement of some Mn with Ti and Mg has increased stability,<sup>14,18,19</sup> but fundamental stabilizing mechanism and energetics are not well-known. Since the aforementioned phase changes are also a problem

when trying to perform high-temperature measurements, one of the aims of this study is to investigate the thermodynamic properties of orthorhombic CaMnO<sub>3-δ</sub>, with different levels of oxygen vacancies, using density functional theory (DFT). Another point to make is the fact that there is currently a discrepancy between theoretical and experimental data when it comes to CaMnO<sub>3-δ</sub>. Estimates obtained by combining a semiempirical model proposed by Goldyeva et al.<sup>20</sup> with either a commonly used data source, FactSage, or experimental measurements by Rørmark et al.<sup>21</sup> and Bakken et al.,<sup>22</sup> yield very different results.<sup>23</sup> This discrepancy, the fact that this system has shown promise as an oxygen carrier, that it can be modified in many ways, and that the fundamental properties are not well understood warrants a deeper study.

The method employed in this study has previously been used to estimate properties of mixed metal oxides and displayed good agreement with experimental data.<sup>23</sup> This approach should be regarded as state-of-the-art when it comes to estimating thermodynamic properties. Since it only relies on a combination of DFT calculations and tabulated data for well-known oxides, it is possible to explore previously unknown systems and compositions of novel materials. This approach can be especially interesting for complex oxides, like perovskites, where relevant data may be difficult to obtain experimentally due to the nonstoichiometric behavior of such materials.<sup>24</sup> As far as we know, this is the first time this method has been used to investigate perovskite materials and the effect of oxygen vacancies.

## 2. METHODS

The study uses a method previously presented by Brorsson et al.<sup>23</sup> but with the addition of accounting for oxygen vacancies in the studied material. The method, which is presented in Figure 1, was originally proposed by Benisek and Dachs<sup>25</sup> and is based on DFT calculations. Generally, the starting point is the crystal structure of the material of interest. After using DFT to find the lowest energy state, it is possible to estimate the phononic contribution of the heat capacity based on the harmonic approximation. When combined with the 0 K energies from the DFT calculations, an estimation of the reaction enthalpy at 298.15 K can be obtained. By using the results together with tabulated thermodynamic properties of well-known simple metal oxides, it is possible to determine the temperature dependent specific heat capacity together with the entropy and the formation enthalpy at 298.15 K.

For a crystal in which multiple species, including vacancies, occupy the same lattice sites, a method called cluster expansion (CE) can be trained in order to find the ground state.<sup>26</sup> Otherwise, the method is the same as that employed for systems with only one species per lattice site. In the former case, it is also possible to use the CE to perform Monte Carlo simulations and thereby estimate the contribution of chemical ordering to the heat capacity. All these steps are explained in more detail in the following sections.

**2.1. Procedure and Theory.** The procedure used here involves the following steps.

1. Identify a chemical reaction describing the formation of the studied metal oxide from a set of binary oxides for which thermodynamic data is available. The current study investigated CaMnO<sub>3-δ</sub> and the simple metal oxides utilized to calculate the formation energy were

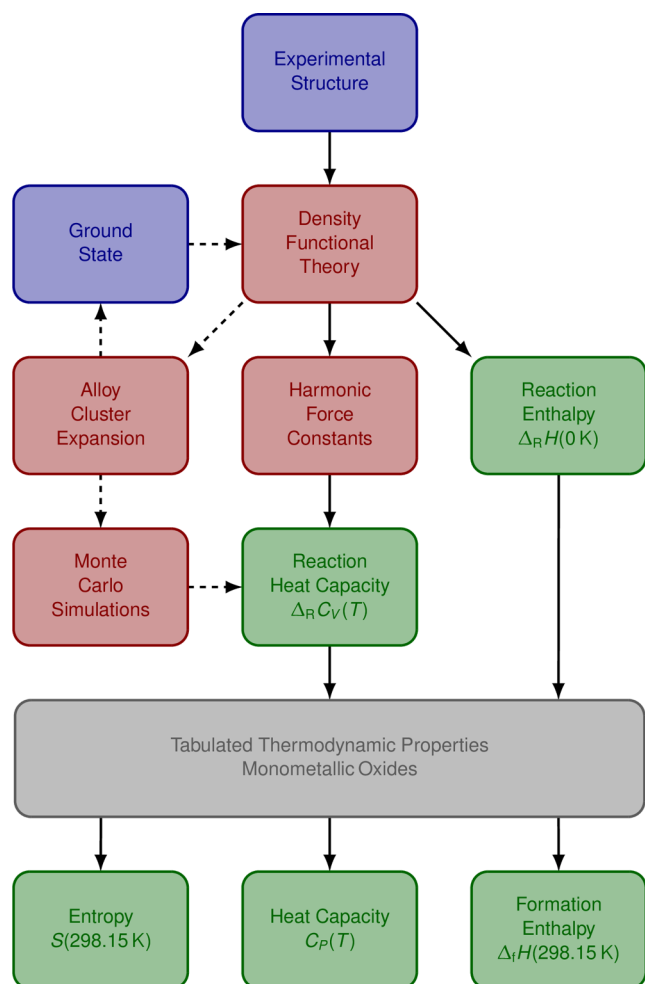
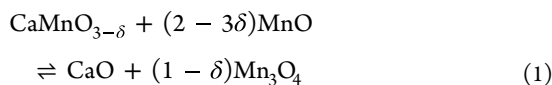


**Figure 1.** Schematic illustration of the procedure for estimating the entropy, formation enthalpy, and heat capacity by combining first-principles calculations and tabulated experimental data for monometallic oxides. Specifically, the main (optional) steps are indicated by the solid (dashed) arrows, while the blue, orange, and green blocks represent external data, computational methods, and results, respectively. The optional steps are only required when the ground state of the material is not known, which is the case for structures with vacancies.

CaO, Mn<sub>3</sub>O<sub>4</sub> and MnO. The theoretical reaction is shown in eq 1



2. Calculate the heat capacity for the reaction at constant volume

$$\Delta_{\text{R}} C_{\text{V}} = C_{\text{V,CaMnO}_{3-\delta}} - (C_{\text{V,CaO}} + (1 - \delta)C_{\text{V,Mn}_3\text{O}_4} - (2 - 3\delta)C_{\text{V,MnO}}) \quad (2)$$

3. Assume that the heat of reaction at 0 K can be represented by the change in internal energy

$$\begin{aligned} \Delta_{\text{R}} H^{0\text{K}} &= \Delta_{\text{R}} U^{0\text{K}} + P\Delta_{\text{R}} V^{0\text{K}} \approx \Delta_{\text{R}} U^{0\text{K}} \\ &= U_{\text{CaMnO}_{3-\delta}}^{0\text{K}} - (U_{\text{CaO}}^{0\text{K}} + (1 - \delta)U_{\text{Mn}_3\text{O}_4}^{0\text{K}} \\ &\quad - (2 - 3\delta)U_{\text{MnO}}^{0\text{K}}) \end{aligned} \quad (3)$$

4. Estimate the enthalpy and entropy of the reaction at room temperature

$$\Delta_{\text{R}} H^{298.15\text{K}} \approx \Delta_{\text{R}} H^{0\text{K}} + \int_0^{298.15} \Delta_{\text{R}} C_{\text{V}} dT \quad (4)$$

$$\Delta_{\text{R}} S^{298.15\text{K}} \approx \Delta_{\text{R}} S^{0\text{K}} + \int_0^{298.15} \frac{\Delta_{\text{R}} C_{\text{V}}}{T} dT \quad (5)$$

5. Use experimental data for the monometallic oxides to correct the formation enthalpy and entropy of the studied metal oxide

$$\begin{aligned} \Delta_{\text{f}} H^{298.15\text{K}} &= \Delta_{\text{R}} H^{298.15\text{K}} + \Delta_{\text{R}} H_{\text{CaO}}^{298.5\text{K}} \\ &\quad + (1 - \delta)\Delta_{\text{f}} H_{\text{Mn}_3\text{O}_4}^{298.5\text{K}} \\ &\quad - (2 - 3\delta)\Delta_{\text{f}} H_{\text{MnO}}^{298.5\text{K}} \end{aligned} \quad (6)$$

$$\begin{aligned} S^{298.15\text{K}} &= \Delta_{\text{R}} S^{298.15\text{K}} + S_{\text{CaO}}^{298.15\text{K}} + (1 - \delta)S_{\text{Mn}_3\text{O}_4}^{298.15\text{K}} \\ &\quad - (2 - 3\delta)S_{\text{MnO}}^{298.15\text{K}} \end{aligned} \quad (7)$$

While Benisek and Dachs only used the above procedure to estimate properties at room temperature, Brorsson et al.<sup>23</sup> showed how this approach can be extended to include the heat capacity at elevated temperatures. Specifically, it is assumed that the following two expressions of the enthalpy of formation are equal

$$\Delta_{\text{f}} H^T = \Delta_{\text{f}} H^{0\text{K}} + \int_0^T C_{\text{p}} dT' \quad (8)$$

$$\begin{aligned} \Delta_{\text{f}} H^T &\approx \Delta_{\text{R}} H^{0\text{K}} + \int_0^T \Delta_{\text{R}} C_{\text{V}} dT' + \Delta_{\text{f}} H_{\text{CaO}}^T \\ &\quad + (1 - \delta)\Delta_{\text{f}} H_{\text{Mn}_3\text{O}_4}^T - (2 - 3\delta)\Delta_{\text{f}} H_{\text{MnO}}^T \end{aligned} \quad (9)$$

which leads to the following expression for the heat capacity

$$\begin{aligned} \int_0^T C_{\text{p}} dT' &\approx \Delta_{\text{R}} H^{0\text{K}} + \int_0^T \Delta_{\text{R}} C_{\text{V}} dT' + \Delta_{\text{f}} H_{\text{CaO}}^T \\ &\quad + (1 - \delta)\Delta_{\text{f}} H_{\text{Mn}_3\text{O}_4}^T - (2 - 3\delta)\Delta_{\text{f}} H_{\text{MnO}}^T \\ &\quad - \Delta_{\text{f}} H^{0\text{K}} \end{aligned} \quad (10)$$

Crucially, tabulated reference data for the monometallic oxides is used to increase the accuracy. The reference data for CaO was taken from the NIST-JANAF thermochemical tables, and the data for Mn<sub>3</sub>O<sub>4</sub> and MnO from other publications.<sup>27,28</sup> Since the formation enthalpies are given by

$$\Delta_{\text{f}} H_{\text{X}}^T = \Delta_{\text{f}} H_{\text{X}}^0 + \int_0^T C_{\text{p,X}} dT' \quad (11)$$

where X = CaO, Mn<sub>3</sub>O<sub>4</sub>, and MnO, the expression for the heat capacity, of the compound of interest, in eq 10 can be reduced to

$$C_p(T) = \Delta_R C_V(T) + C_{p,\text{CaO}}(T) + (1 - \delta)C_{p,\text{Mn}_3\text{O}_4}(T) - (2 - 3\delta)C_{p,\text{MnO}}(T) \quad (12)$$

To use the results together with other components and phases, such as the FactSage software, it is necessary to express the specific heat capacity, at constant pressure, as a function of temperature using a series of power functions with a maximum of eight terms

$$C_p(T) = \sum_{i=1}^8 k_i T^i \quad (13)$$

In this study, five terms were used to estimate the heat capacity of  $\text{CaMnO}_{3-\delta}$

$$C_p(T) = k_0 + k_1 T^{-0.5} + k_2 T^{-3} + k_3 T^{-2} + k_4 T^{-1} \quad (14)$$

**2.2. Representative Structure.** Structures collected from the Materials Project<sup>29</sup> were used as starting points for the first-principles calculations. Since only stoichiometric  $\text{CaMnO}_3$  is found in said database, the ground states for compositions with oxygen vacancies were determined using CEs.

**2.3. Ground State from Cluster Expansions.** The ICET toolkit<sup>30</sup> was used to find the ground states of structures with oxygen vacancies via the creation of alloy CEs. This method is often used to represent disordered systems as combinations of clusters with different symmetries. Based on the order, or in other words, the number of atoms, these clusters can be classified as pairs, triplets, quadruplets, and so on. Since the number of clusters is theoretically infinite, those above a certain order or with radii larger than specific cutoffs are disregarded. In practice, however, the selection is often limited by the available computational resources as well as the size of the training data set.

Here, 200 configurations were created by randomly replacing oxygen atoms in 80 atom  $\text{CaMnO}_3$  supercells with vacancies. After relaxing the structures as detailed below, a CE, with cutoffs of 3.5 Å for pairs and 1.5 Å for triplets, was fitted using automatic relevance detection regression (ARDR). The ground states were then determined using a procedure based on multiple integer programming that is implemented in ICET.<sup>30</sup>

The alloy CE was also used to estimate the contribution to the heat capacity from the chemical ordering, specifically by performing Monte Carlo (MC) simulations using the MCHAMMER module of ICET.<sup>30</sup>

**2.4. Computational Details.** DFT, as implemented in VASP<sup>31</sup> (version 5.4.4), was used for all first-principles calculations required to evaluate (eqs 2–5), which includes structure relaxations and force determinations. The input files were, more precisely, generated with PYMATGEN.<sup>32</sup> This ensured that the settings were the same as in the Materials Project,<sup>29</sup> which entailed using the generalized gradient approximation (GGA) functionals presented by Perdew, Burke and Ernzerhof (PBE)<sup>33</sup> and an energy cutoff of 520 eV as well as setting the  $U$ -value for Mn to 3.9 eV.<sup>32</sup> Initially, the energy difference for the electronic and ionic convergence was set to  $10^{-3}$  and  $10^{-2}$  eV per atom, respectively. After this, a second relaxation was performed using the same functionals, to achieve more accurate results, where the same thresholds were set to  $10^{-6}$  and  $10^{-5}$  eV. In addition, structure relaxations using SCAN and  $r^2$ SCAN functionals were done for stoichiometric  $\text{CaMnO}_3$ . Specifically, the purpose was to determine the

difference in free energy when using more detailed functionals than GGA +  $U$ .

To generate a reciprocal grid of  $k$ -points, the Monkhorst–Pack method was used for the stoichiometric  $\text{CaMnO}_3$ . For each oxygen vacancy concentration, the  $\gamma$ -centered method was used. A reciprocal grid of 1100  $k$ -points per atom was used, which is higher than the default setting in the Materials Project (1000). The tetrahedron method with Blöchl correction was used to sample the grid for all compositions.

This study concerns the following compositions with different fractions of vacancies:  $\text{CaMnO}_3$ ,  $\text{CaMnO}_{2.9375}$ ,  $\text{CaMnO}_{2.875}$ ,  $\text{CaMnO}_{2.8125}$ ,  $\text{CaMnO}_{2.75}$ ,  $\text{CaMnO}_{2.6875}$ ,  $\text{CaMnO}_{2.625}$ ,  $\text{CaMnO}_{2.5625}$ ,  $\text{CaMnO}_{2.5}$ . In the case of stoichiometric  $\text{CaMnO}_3$ , calculations were performed on the primitive orthorhombic unit cell with 20 atoms,  $\text{Ca}_4\text{Mn}_4\text{O}_{12}$ . To represent different oxygen vacancy concentrations, meanwhile, unit cells with up to 79 atoms had to be used, specifically  $\text{Ca}_{16}\text{Mn}_{16}\text{O}_{47}$ ,  $\text{Ca}_{16}\text{Mn}_{16}\text{O}_{46}$ ,  $\text{Ca}_{16}\text{Mn}_{16}\text{O}_{45}$ ,  $\text{Ca}_{16}\text{Mn}_{16}\text{O}_{44}$ ,  $\text{Ca}_{16}\text{Mn}_{16}\text{O}_{43}$ ,  $\text{Ca}_{16}\text{Mn}_{16}\text{O}_{42}$ ,  $\text{Ca}_{16}\text{Mn}_{16}\text{O}_{41}$ , and  $\text{Ca}_{16}\text{Mn}_{16}\text{O}_{40}$ .

**2.5. Phononic Heat Capacity.** The phononic contribution to the heat capacity was estimated using the PHONOPY<sup>34</sup> package based on force constants (FCs) that were determined using HIPHIVE.<sup>26</sup> Fifteen “rattled” supercells, with up to 210 atoms, were generated from the ground state structure for each oxygen vacancy concentration by randomly displacing all atoms by distances drawn from a Gaussian distribution with a 0.02 Å standard deviation. Note that the primitive unit cell was repeated the same number of times for all vacancy concentrations. In the case of  $\text{Ca}_{16}\text{Mn}_{16}\text{O}_{47}$ , for instance, the supercells consisted of 158 atoms compared to 200 for  $\text{CaMnO}_3$ . The interatomic forces, obtained from a static calculation in VASP, were used, together with the displacements, to fit the force constant potentials (FCPs). By using the force constants (FCs) extracted from the FCPs, the heat capacity, entropy, and free energy were calculated from 10 K up to 2500 K based on a uniform mesh with  $5 \times 10^6$   $q$ -points per reciprocal atom.

**2.6. Generation of Phase Diagrams.** The Ca–Mn–O system was evaluated using FactSage 8.2,<sup>35</sup> which determines chemical equilibrium by minimizing the Gibbs free energy while considering thermodynamic data for selected phases and compounds. In particular, this work involved the use of the FactPS and FToxid databases, for pure substances and oxide solutions, respectively, as well as semiempirical data.<sup>36</sup> Additionally, data obtained from the first-principles calculations for each of the eight different nonstoichiometric  $\text{CaMnO}_{3-\delta}$  phases were incorporated into a user-defined database. More specifically, this included the formation enthalpy and entropy at room temperature, together with the coefficients in the power series representation of the heat capacity in eq 14.

The stability of  $\text{CaMnO}_{3-\delta}$  under CLC-conditions was analyzed by comparing Gibbs free energies and involved generating phase diagrams for an equimolar mixture of Ca and Mn, oxygen partial pressures between 1 atm and  $10^{-12}$  atm, and temperatures ranging from 100 to 1200 °C.

## 3. RESULTS AND DISCUSSION

**3.1. Calculated Thermal Properties.** By applying the method described in the previous section, the coefficients in the expression for the heat capacity in eq 14 were determined for each oxygen vacancy concentration. The enthalpy of

**Table 1. Thermodynamic Properties of Structures with Different Oxygen Vacancy Concentrations Based on GGA + *U* Calculations<sup>a</sup>**

system	$\Delta_f H^{298.15K}$ [kJ/mol]	$S^{298.15K}$ [J/molK]	$k_0$ [J/molK]	$k_1$ [J/molK <sup>0.5</sup> ]	$k_2$ [J/mol]	$k_3$ [JK/mol]	$k_4$ [JK <sup>2</sup> /mol]
CaMnO <sub>2.5</sub>	$-1.092 \times 10^6$	100.03	94.26	$4.72 \times 10^3$	$-153.19 \times 10^3$	$34.28 \times 10^6$	$-4.06 \times 10^9$
CaMnO <sub>2.5625</sub>	$-1.112 \times 10^6$	98.49	19.11	$11.47 \times 10^3$	$-320.98 \times 10^3$	$69.15 \times 10^6$	$-7.93 \times 10^9$
CaMnO <sub>2.625</sub>	$-1.134 \times 10^6$	100.08	48.58	$9.37 \times 10^3$	$-269.19 \times 10^3$	$58.28 \times 10^6$	$-6.73 \times 10^9$
CaMnO <sub>2.6875</sub>	$-1.138 \times 10^6$	97.22	-34.96	$16.66 \times 10^3$	$-446.74 \times 10^3$	$93.99 \times 10^6$	$-10.60 \times 10^9$
CaMnO <sub>2.75</sub>	$-1.149 \times 10^6$	99.55	24.41	$11.95 \times 10^3$	$-333.78 \times 10^3$	$71.49 \times 10^6$	$-8.18 \times 10^9$
CaMnO <sub>2.8125</sub>	$-1.160 \times 10^6$	98.76	-45.48	$18.10 \times 10^3$	$-481.83 \times 10^3$	$100.53 \times 10^6$	$-11.27 \times 10^9$
CaMnO <sub>2.875</sub>	$-1.168 \times 10^6$	95.79	-14.01	$15.57 \times 10^3$	$-424.29 \times 10^3$	$90.14 \times 10^6$	$-10.24 \times 10^9$
CaMnO <sub>2.9375</sub>	$-1.179 \times 10^6$	93.48	-34.61	$17.49 \times 10^3$	$-471.24 \times 10^3$	$99.43 \times 10^6$	$-11.25 \times 10^9$
CaMnO <sub>3</sub>	$-1.189 \times 10^6$	96.32	-46.62	$19.18 \times 10^3$	$-514.48 \times 10^3$	$108.49 \times 10^6$	$-12.26 \times 10^9$

<sup>a</sup>The formation enthalpy ( $\Delta_f H^{298.15K}$ ) and entropy ( $S^{298.15K}$ ) were calculated using eqs 6 and 7. The coefficients for eq 14 for each structure are also presented.

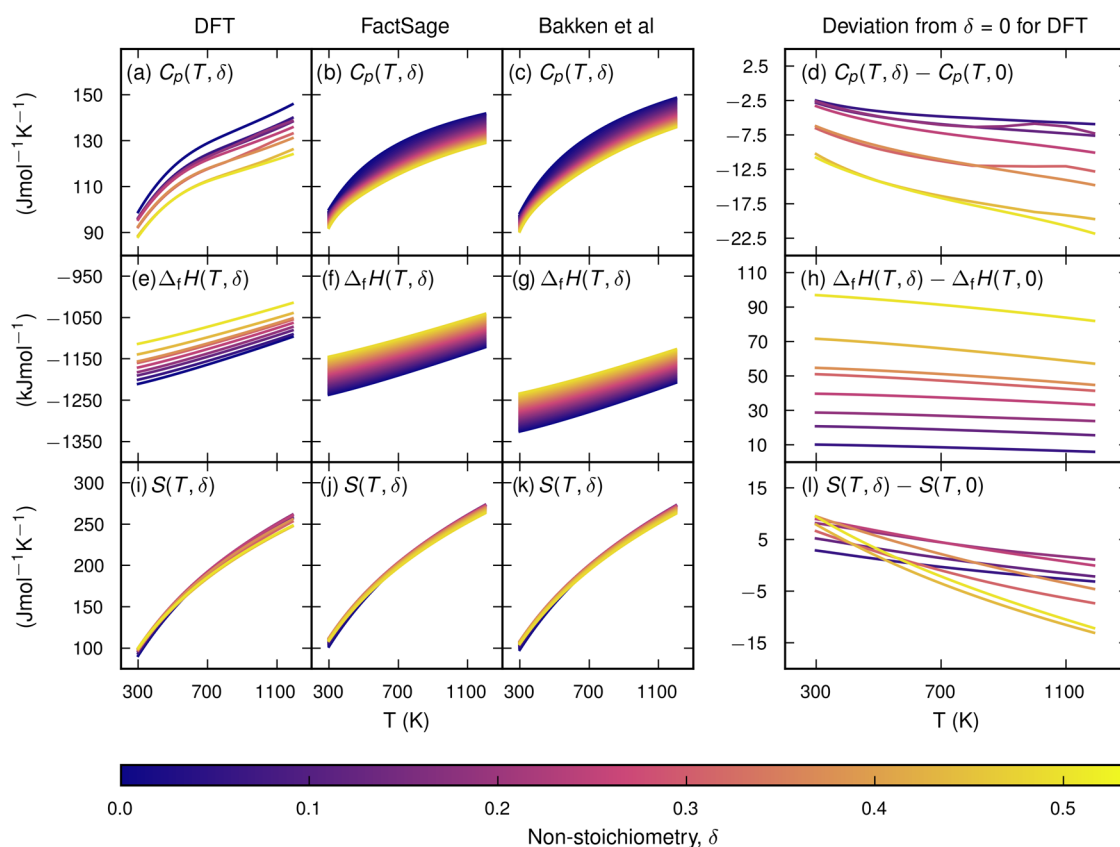


**Figure 2.** Heat capacity (a–d), formation enthalpy (e–h), and entropy (i–l) from DFT calculations (a, e, i) as well as a semiempirical model combined with experimental data from either FactSage (b, f, j) or Rørmark et al. and Bakken et al. (c, g, k). The panels in the leftmost column (d, h, l) show the deviation between  $\delta = 0$  and  $\delta > 0$ .

formation and entropy, both at room temperature, were also estimated and are presented in Table 1.

The plots of the heat capacity, shown in Figure 2, for the different vacancy concentrations in Table 1 show that the computational results presented in this work (DFT) are in good agreement with data obtained by using experimental data from Factsage, or Rørmark et al.<sup>21</sup> and Bakken et al.,<sup>22</sup> together with a semiempirical model proposed by Goldyeva et al.<sup>20</sup> While the first-principles calculations yield a wider spread in the heat capacity when comparing the different vacancy concentrations, the overall behavior is similar. As expected, the heat capacity decreases as the number of vacancies increases, since there are fewer atoms per formula unit. Even so, it is possible to discern some unique behavior for individual

vacancy concentrations. For instance, some show a sharper increase in heat capacity at around 800 K. This is a direct effect of chemical ordering, specifically in the form of an order–disorder transition that leads to an abrupt increase in the heat capacity. Since the transition temperatures differ depending on the vacancy concentration, some occur outside the range displayed in the figure.

Figure 2 clearly shows that the curves corresponding to different vacancy concentrations have similar shapes for all properties and data sets. Still, there is a slight difference in relative values. In this study, the heat capacity, enthalpy of formation and entropy differ from the FactSage data by +0.77 J/(molK), +48 kJ/mol, and -5.43 J/(molK) at 298.15 K and  $\delta = 0$  when using GGA + *U* functional. Using the SCAN

functional, these values change to  $-1.17$  J/(molK),  $+26$  kJ/mol, and  $-11.17$  J/(molK) at 298.15 K and  $\delta = 0$ . When compared with the data based on Rørmark et al.<sup>21</sup> and Bakken et al.<sup>22</sup> the differences in the same properties are  $+0.44$  J/(molK),  $+115$  kJ/mol, and  $-7.24$  J/(molK) using the SCAN functional. The difference between results from SCAN and  $r^2$ SCAN is within 0.5%.

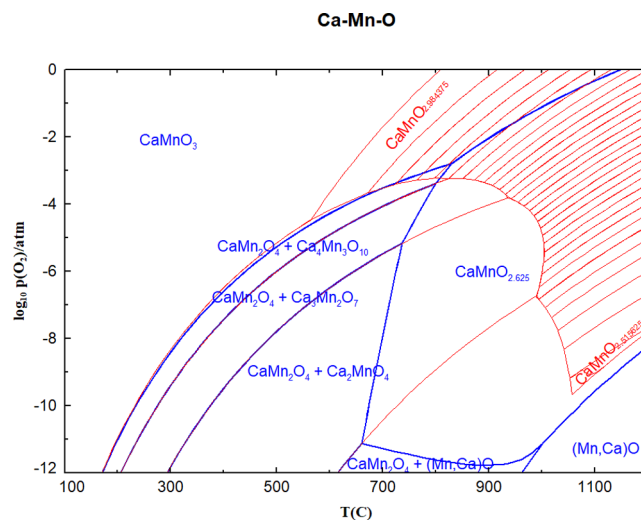
It can be concluded that the calculated heat capacity and entropy are well within the experimental margin of error ( $\pm 10\%$ ). The formation enthalpies obtained from first-principles indicate that  $\text{CaMnO}_{3-\delta}$  is significantly less stable compared to the experimental data, however. Even so, it is worth noting that the difference between the results from this study and FactSage is less than  $\pm 10\%$ . For comparison with Rørmark et al.<sup>21</sup> and Bakken et al.<sup>22</sup> the difference is close to  $\pm 10\%$ .

There are many potential explanations for the discrepancy between the computational results and experiments. First the experimental data represents a combination of measurements from two separate studies.<sup>21,22</sup> Specifically, the enthalpy of formation at room temperature was estimated by taking the value for  $\text{CaMnO}_{2,996}$  at 993 K reported by Rørmark et al.<sup>21</sup> and subtracting the enthalpy change obtained by integrating the heat capacity measured by Bakken et al.<sup>22</sup> from 298.15 to 993 K. Note that the latter data only extends to 650 K, since  $\text{CaMnO}_3$  was found to decompose above this temperature, and a piecewise cubic hermite interpolating polynomial (PCHIP) was therefore used for extrapolation up to 993 K. Another possible explanation for the lack of agreement could be that the materials used in previous experiments did not correspond to pure  $\text{CaMnO}_3$ , but instead a mixture of various structurally related phases with similar X-ray diffraction spectra, i.e., incorporation of minor amounts of impurities on the A- or B-site, perhaps not discernible in XRD spectra. These might have lower formation enthalpies, which would lead to an underestimation of the value for pure  $\text{CaMnO}_3$ . It should be noted that in experiments with chemical-looping using  $\text{CaMnO}_3$ , phase diagrams of used materials almost always contain some other phases,  $\text{Ca}_2\text{MnO}_4$  or  $\text{CaMn}_2\text{O}_4$ , which could suggest that  $\text{CaMnO}_3$  is unstable during the process.<sup>36</sup> Moreover, the sizes of the supercells, which were chosen to keep the computational load manageable, could have an effect on the results. As was also noted, the structure of the crystal is orthorhombic. While this is the most stable structure at 0 K for stoichiometric  $\text{CaMnO}_3$ , it will change at higher temperatures and vacancy concentrations.<sup>36</sup> New calculations would have to be performed for these alternative crystal symmetries to see if there are any effects on the thermodynamic properties as calculated in this work. This direction for further investigation forms part of our future research plans, but it lies beyond the scope of the present study.

**3.2. Elucidating the Effect of Oxygen Vacancies.** If the results from this study are combined with the data in the FactSage database to create a phase diagram, the stability of  $\text{CaMnO}_{3-\delta}$  is too low for this phase to be visible. This is not unexpected, however, since the formation enthalpy for  $\text{CaMnO}_3$  is predicted to be 26 kJ/mol higher than the value in the FactSage database when using SCAN or  $r^2$ SCAN as the functional and 48 kJ/mol when using GGA +  $U$ , as was mentioned in the previous section.

To model the effect of oxygen vacancies, the calculated formation enthalpies were, thus, shifted by the difference for stoichiometric  $\text{CaMnO}_3$  relative to the data in FactSage at

298.15 K. By using the resulting estimates, together with the data for other phases from the FactPS and FToxid databases, it is possible to construct a more complete diagram, which is marked by blue lines in Figure 3. The results obtained in this



more than 80 atoms. If it would be possible to study larger unit cells, and therefore a finer grid of oxygen vacancies, the results can be expected to show a clearer transition between the phases in the phase diagram. It should also be stressed that the data from Figure 3 is shown to give a more explicit view of the influence of oxygen vacancies, which was the purpose of developing this novel method of estimating the thermodynamic properties for OCs, and that the enthalpy was adjusted to reflect data available in the FactSage databases.

Still, the analysis shows that there are significant discrepancies with respect to the ground state energy of different sources. From the current study, it is suggested that the pure  $\text{CaMnO}_3$  system may not be as stable as previously determined, but further investigations and comparisons are necessary.

#### 4. CONCLUSIONS

This study shows that a semiempirical method, which is based on a combination of DFT and harmonic phonon calculations, can be used to estimate the thermodynamic properties of complex metal oxides, here in the form of the OC material  $\text{CaMnO}_{3-\delta}$ . A key achievement of this work is the expansion of the phase diagram for the Ca–Mn–O system, incorporating detailed data on oxygen vacancies. This novel approach allows for a deeper understanding of the influence of oxygen vacancies on the thermodynamic properties and phase stability of  $\text{CaMnO}_{3-\delta}$ , which is critical for its performance in CLC. The heat capacity and entropy calculated in this study are determined to be within the experimental margin of error of ( $\pm 10\%$ ). The resulting Ca–Mn–O phase diagram shows that the  $\text{CaMnO}_{2.625}$  phase is the most thermodynamically stable at high temperatures and oxygen partial pressures. However, our results also indicate that stoichiometric  $\text{CaMnO}_3$  is less stable than previously proposed in literature. This discrepancy between calculated and experimental data warrants further investigation to identify the exact cause.

The ability to create a new phase diagram based on detailed data for oxygen vacancies represents a significant advancement. This method enables the exploration of complex novel materials for use in CLC processes, providing valuable insights into the correlation between inherent properties and OC capacity. Additionally, individual phases that are difficult or even impossible to isolate and test experimentally can be investigated using this methodology, paving the way for future material exploration and development.

#### ■ AUTHOR INFORMATION

##### Corresponding Author

**Jonatan Gastaldi** – Department of Space, Earth, and Environment, Division of Energy Technology, Chalmers University of Technology, Gothenburg SE-41296, Sweden; [orcid.org/0009-0006-4948-2209](https://orcid.org/0009-0006-4948-2209); Email: [gastaldi@chalmers.se](mailto:gastaldi@chalmers.se)

##### Authors

**Joakim Brorsson** – Department Physics, Division of Chemical Physics, Chalmers University of Technology, Gothenburg SE-41296, Sweden

**Ivana Staničić** – Department of Space, Earth, and Environment, Division of Energy Technology, Chalmers University of Technology, Gothenburg SE-41296, Sweden; [orcid.org/0000-0002-6927-4822](https://orcid.org/0000-0002-6927-4822)

**Anders Hellman** – Department Physics, Division of Chemical Physics, Chalmers University of Technology, Gothenburg SE-41296, Sweden; [orcid.org/0000-0002-1821-159X](https://orcid.org/0000-0002-1821-159X)

**Tobias Mattisson** – Department of Space, Earth, and Environment, Division of Energy Technology, Chalmers University of Technology, Gothenburg SE-41296, Sweden; [orcid.org/0000-0003-3942-7434](https://orcid.org/0000-0003-3942-7434)

Complete contact information is available at: <https://pubs.acs.org/10.1021/acs.energyfuels.5c00267>

#### Author Contributions

J.G.: Conceptualization; visualization; writing—original draft. J.B.: Conceptualization; writing—review and editing. I.S.: Visualization; writing—review and editing. A.H.: Supervision; writing—review and editing; supervision. T.M.: Supervision; writing—review and editing.

#### Notes

The authors declare no competing financial interest.

#### ■ ACKNOWLEDGMENTS

This work was funded by the Swedish Research Council through grant agreement no. 2020-03487 and the computations were enabled by resources provided by the National Academic Infrastructure for Supercomputing in Sweden (NAISS) at NSC and PDC through projects 2023/3-29, 2023/5-147, 2023/5-521, 2024/5-260.

#### ■ REFERENCES

- (1) Lee, H.; Calvin, K.; Dasgupta, D. et al. *Climate Change 2023: Synthesis Report. Contribution of Working Groups I, II and III to the Sixth Assessment Report of the Intergovernmental Panel on Climate Change*; The Australian National University, 2023.
- (2) UNFCCC. *Paris Climate Change Conference - November 2015*, "Presented at the COP 21, Paris, 2018.
- (3) Gasser, T.; Guivarch, C.; Tachiiri, K.; Jones, C. D.; Ciais, P. Negative emissions physically needed to keep global warming below 2 C. *Nat. Commun.* **2015**, *6* (1), No. 7958.
- (4) Fuss, S.; Canadell, J. G.; Peters, G. P.; et al. Betting on negative emissions. *Nat. Clim. Change* **2014**, *4* (10), 850–853.
- (5) Azar, C.; Lindgren, K.; Obersteiner, M.; et al. The feasibility of low CO<sub>2</sub> concentration targets and the role of bio-energy with carbon capture and storage (BECCS). *Clim. Change* **2010**, *100*, 195–202.
- (6) Bartocci, P.; Abad, A.; Flores, A. C.; de las Obras Loscertales, M. Ilmenite: A promising oxygen carrier for the scale-up of chemical looping. *Fuel* **2023**, *337*, No. 126644.
- (7) Leion, H.; Lyngfelt, A.; Johansson, M.; Jerndal, E.; Mattisson, T. The use of ilmenite as an oxygen carrier in chemical-looping combustion. *Chem. Eng. Res. Des.* **2008**, *86* (9), 1017–1026.
- (8) Jerndal, E.; Mattisson, T.; Lyngfelt, A. Thermal analysis of chemical-looping combustion. *Chem. Eng. Res. Des.* **2006**, *84* (9), 795–806.
- (9) Linderholm, C.; Lyngfelt, A.; Cuadrat, A.; Jerndal, E. Chemical-looping combustion of solid fuels—Operation in a 10 kW unit with two fuels, above-bed and in-bed fuel feed and two oxygen carriers, manganese ore and ilmenite. *Fuel* **2012**, *102*, 808–822.
- (10) Arjmand, M.; Leion, H.; Mattisson, T.; Lyngfelt, A. Investigation of different manganese ores as oxygen carriers in chemical-looping combustion (CLC) for solid fuels. *Appl. Energy* **2014**, *113*, 1883–1894.
- (11) Rydén, M.; Leion, H.; Mattisson, T.; Lyngfelt, A. Combined oxides as oxygen-carrier material for chemical-looping with oxygen uncoupling. *Appl. Energy* **2014**, *113*, 1924–1932.

- (12) Mattisson, T. Materials for Chemical-Looping with Oxygen Uncoupling. In *International Scholarly Research Notices*; Wiley, 2013; Vol. 2013.
- (13) Arjmand, M.; Azad, A.-M.; Leion, H.; Lyngfelt, A.; Mattisson, T. Prospects of  $\text{Al}_2\text{O}_3$  and  $\text{MgAl}_2\text{O}_4$ -supported  $\text{CuO}$  oxygen carriers in chemical-looping combustion (CLC) and chemical-looping with oxygen uncoupling (CLOU). *Energy Fuels* **2011**, *25* (11), 5493–5502.
- (14) Rydén, M.; Lyngfelt, A.; Mattisson, T.  $\text{CaMn}_0.875\text{Ti}_0.125\text{O}_3$  as oxygen carrier for chemical-looping combustion with oxygen uncoupling (CLOU)—Experiments in a continuously operating fluidized-bed reactor system. *Int. J. Greenhouse Gas Control* **2011**, *5* (2), 356–366.
- (15) Hallberg, P.; Jing, D.; Rydén, M.; Mattisson, T.; Lyngfelt, A. Chemical Looping Combustion and Chemical Looping with Oxygen Uncoupling Experiments in a Batch Reactor Using Spray-Dried  $\text{CaMn}_{1-x}\text{M}_x\text{O}_{3-\delta}$  ( $M = \text{Ti, Fe, Mg}$ ) Particles as Oxygen Carriers. *Energy Fuels* **2013**, *27* (3), 1473–1481.
- (16) Chen, Y.; Galinsky, N.; Wang, Z.; Li, F. Investigation of perovskite supported composite oxides for chemical looping conversion of syngas. *Fuel* **2014**, *134*, 521–530.
- (17) Dai, X. P.; Li, J.; Fan, J. T.; Wei, W. S.; Xu, J. Synthesis gas generation by chemical-looping reforming in a circulating fluidized bed reactor using perovskite  $\text{LaFeO}_3$ -based oxygen carriers. *Ind. Eng. Chem. Res.* **2012**, *51* (34), 11072–11082.
- (18) Leion, H.; Larring, Y.; Bakken, E.; Bredesen, R.; Mattisson, T.; Lyngfelt, A. Use of  $\text{CaMn}_0.875\text{Ti}_0.125\text{O}_3$  as oxygen carrier in chemical-looping with oxygen uncoupling. *Energy Fuels* **2009**, *23* (10), 5276–5283.
- (19) Schmitz, M.; Linderholm, C. J. Performance of calcium manganate as oxygen carrier in chemical looping combustion of biochar in a 10 kW pilot. *Appl. Energy* **2016**, *169*, 729–737.
- (20) Goldyreva, E. I.; Leonidov, I. A.; Patrakeev, M. V.; Kozhevnikov, V. L. "Thermodynamics of oxygen in  $\text{CaMnO}_{3-\delta}$ ". *J. Solid State Electrochem.* **2013**, *17*, 3185–3190.
- (21) Rørmark, L.; Stølen, S.; Wiik, K.; Grande, T. Enthalpies of formation of  $\text{La}_{1-x}\text{A}_x\text{MnO}_3 \pm \delta$  ( $A = \text{Ca and Sr}$ ) measured by high-temperature solution calorimetry. *J. Solid State Chem.* **2002**, *163* (1), 186–193.
- (22) Bakken, E.; Boerio-Goates, J.; Grande, T.; et al. "Entropy of oxidation and redox energetics of  $\text{CaMnO}_{3-\delta}$ ". *Solid State Ionics* **2005**, *176* (29–30), 2261–2267.
- (23) Brorsson, J.; Staničić, I.; Gastaldi, J.; Mattison, T.; Hellman, A. Thermodynamic properties for metal oxides from first-principles. *Comput. Mater. Sci.* **2024**, *233*, No. 112690.
- (24) Wang, J.; Mueller, D. N.; Crumlin, E. J. Recommended strategies for quantifying oxygen vacancies with X-ray photoelectron spectroscopy. *J. Eur. Ceram. Soc.* **2024**, *44*, No. 116709.
- (25) Benisek, A.; Dachs, E. The accuracy of standard enthalpies and entropies for phases of petrological interest derived from density-functional calculations. *Contrib. Mineral. Petrol.* **2018**, *173*, No. 90.
- (26) Eriksson, F.; Fransson, E.; Erhart, P. The Hiphive Package for the extraction of high-order force constants by machine learning. *Adv. Theory Simul.* **2019**, *2* (5), No. 1800184.
- (27) Jacob, K. T.; Kumar, A.; Rajitha, G.; Waseda, Y. Thermodynamic data for  $\text{Mn}_3\text{O}_4$ ,  $\text{Mn}_2\text{O}_3$  and  $\text{MnO}_2$ . *High Temp. Mate. Processes* **2011**, *30* (4), 459–472.
- (28) Jacob, K. T.; Kumar, A.; Waseda, Y. Gibbs energy of formation of  $\text{MnO}$ : measurement and assessment. *J. Phase Equilib. Diffus.* **2008**, *29* (3), 222–230.
- (29) Jain, A.; Ong, S. P.; Hautier, G.; et al. Commentary: The Materials Project: A materials genome approach to accelerating materials innovation. *APL Mater.* **2013**, *1*, No. 01002, DOI: [10.1063/1.4812323](https://doi.org/10.1063/1.4812323).
- (30) Ångqvist, M.; Muñoz, W. A.; Rahm, J. M.; et al. ICET—a Python library for constructing and sampling alloy cluster expansions. *Adv. Theory Simul.* **2019**, *2* (7), No. 1900015.
- (31) Kresse, G.; Furthmüller, J. "Efficient iterative schemes for ab initio total-energy calculations using a plane-wave basis set,". *Phys. Rev. B* **1996**, *54* (16), No. 11169.
- (32) Ong, S. P.; Richards, W. D.; Jain, A.; et al. Python Materials Genomics (pymatgen): A robust, open-source python library for materials analysis. *Comput. Mater. Sci.* **2013**, *68*, 314–319.
- (33) Perdew, J. P.; Burke, K.; Ernzerhof, M. Generalized gradient approximation made simple. *Phys. Rev. Lett.* **1996**, *77* (18), No. 3865.
- (34) Togo, A.; Tanaka, I. First principles phonon calculations in materials science. *Scr. Mater.* **2015**, *108*, 1–5.
- (35) Bale, C. W.; Bédise, E.; Chartrand, P.; et al. Reprint of: FactSage thermochemical software and databases, 2010–2016. *Calphad* **2016**, *55*, 1–19.
- (36) Staničić, I.; Brorsson, J.; Hellman, A.; Rydén, M.; Mattisson, T. Thermodynamic analysis on the fate of ash elements in chemical looping combustion of solid fuels—Manganese-Based oxygen carriers. *Fuel* **2024**, *369*, No. 131676.



CAS BIOFINDER DISCOVERY PLATFORM™

**ELIMINATE DATA SILOS. FIND WHAT YOU NEED, WHEN YOU NEED IT.**

A single platform for relevant, high-quality biological and toxicology research

**Streamline your R&D**

CAS  
A Division of the American Chemical Society